Leveraging Automated Machine Learning (AutoML) for Urban Climate Emulation

Junjie Yu[1], Zhonghua Zheng[1,2,3*], Sarah Lindley[4], Lei Zhao[5,6,7], Chi Wang[8], Qingyun Wu[9], Lingcheng Li[10], David O. Topping[1], John S. Schreck[2], David John Gagne[2], Keith W. Oleson[3]

[1]Department of Earth and Environmental Sciences, The University of Manchester, Manchester, M13 9PL, UK.
[2]Computational and Information Systems Laboratory, NSF National Center for Atmospheric Research (NCAR), Boulder, CO 80307, USA.
[3]Climate and Global Dynamics Laboratory, NSF National Center for Atmospheric Research (NCAR), Boulder, CO 80307, USA.
[4]Department of Geography, The University of Manchester, Manchester, M13 9PL, UK.
[5]Department of Civil and Environmental Engineering, University of Illinois Urbana-Champaign, Urbana, IL 61801, USA.
[6]National Center for Supercomputing Applications, University of Illinois Urbana-Champaign, Urbana, IL 61801, USA.
[7]Institute for Sustainability, Energy, and Environment (iSEE), University of Illinois Urbana-Champaign, Urbana, IL 61801, USA.
[8]Google DeepMind, Kirkland, WA 98033, USA.
[9]College of Information Sciences and Technology, Pennsylvania State University, State College, PA 16802, USA.
[10]Atmospheric, Climate, and Earth Sciences Division, Pacific Northwest National Laboratory, Richland, WA 99352, USA.

*Corresponding author(s). E-mail(s): zhonghua.zheng@manchester.ac.uk;
Contributing authors: junjie.yu@postgrad.manchester.ac.uk; sarah.lindley@manchester.ac.uk; leizhao@illinois.edu; wangchi@google.com; qingyun.wu@psu.edu; lingcheng.li@pnnl.gov; david.topping@manchester.ac.uk; schreck@ucar.edu; dgagne@ucar.edu; oleson@ucar.edu;

Abstract

Urban climate models are critical for understanding and addressing the impacts of urban climate change. Yet, process-based urban climate models face limitations of high-entry barriers and substantial computing resource consumption, prompting the development of data-driven methods. However, the recently developed urban climate emulators, being location-dependent, are less scalable and may overlook geospatial data. In this study, we develop location-independent machine learning emulators for the daily maximum canyon air temperature. To overcome the complexities associated with model selection and hyperparameter optimization in machine learning, we apply automated machine learning (AutoML) to emulation tasks and propose a feature importance analysis framework for the AutoML models. By comparing four types of global urban climate emulators, we found that the location information and urban surface parameters can improve the emulation performance. The results of the AutoML tasks demonstrate that AutoML excels in learning the physics-based urban climate model, achieving a root mean squared error (RMSE) of 0.81 Kelvin for emulators parameterized with location information and urban surface parameters, and an RMSE of 0.91 Kelvin in the temporal extrapolation scenario. The feature importance of the emulators indicates that urban morphological parameters contribute more to the emulators than radiative and thermal parameters. The study serves as a demonstration of the potential that AutoML holds for advancing urban climate research and facilitating urban climate modeling.

Keywords: Automated machine learning, Data-driven modeling, Urban climate, Urban surface parameters, Climate change

1 Introduction

Urban areas, which constitute 0.2%–3% of the Earth's land surface (Potere & Schneider, 2007; Schneider, Friedl, & Potere, 2009), now accommodate over 50% of the global population (Ritchie, Samborska, & Roser, 2024). This figure is projected to increase to 68% by 2050 (United Nations, 2019). Such urbanization impacts local meteorology (Dimoudi et al., 2013; Shahrestani et al., 2015; Yang et al., 2024) and air quality (Baklanov et al., 2018; Liang & Gong, 2020; Qi, Che, & Wang, 2023; Zhan et al., 2023), leading to far-reaching socioeconomic (Gasper, Blohm, & Ruth, 2011; Liu, Huang, & Yang, 2020; Romero-Lankao et al., 2018) and ecological (Urban et al., 2024; Zhou et al., 2021) impacts. Under global climate change, it is anticipated that urban areas will be exposed to more severe climate extremes (Ghanbari et al., 2023; J. Wang et al., 2021; Zheng, Zhao, & Oleson, 2021).

Investigating the impacts of climate change in urban areas is crucial for both societal well-being and public health (Dottori et al., 2018; Hu et al., 2023). For example, the urban heat island effect, where urban temperatures exceed those of surrounding areas, can increase mortality risks (Hu et al., 2023). Urbanization changes the land surface and increases anthropogenic heat emissions, making urban climate notably different from other land units. The surface characteristics of urban areas–such as imperviousness, thermal properties, and three-dimensional geometry–change radiation, energy, turbulence and hydrological processes (Hu et al., 2023). These distinct processes in urban areas cannot be adequately simulated without process-based, computational urban climate models.

Extensive efforts have been made to develop computational urban climate models (urban land surface models), which derive their urban-specific simulation outputs (e.g., local urban temperatures) from the interactions between atmospheric forcing and urban surfaces (Lipson et al., 2024). These process-based models enable analysis of how global climate change impacts local urban climates and assist in developing strategies to address extreme urban temperatures, such as implementing white roofs to mitigate urban heat. However, detailed urban climate modeling is often both time-consuming and costly. Additionally, the high computational requirements are further exacerbated by the complexities involved in installing and running these models (Yu et al., 2025). The setup and configuration processes create barriers to entry, particularly for those not specialized in the field. This underscores the critical need for more efficient and accessible urban climate modeling solutions.

Data-driven modeling presents a viable alternative to emulate process-based models and serve as a surrogate. It can harness publicly available model simulation data from projects such as the Community Earth System Model Large Ensemble Community Project (CESM-LE) and Coupled Model Intercomparison Project (CMIP) to train the models. Additionally, data-driven models typically incur lower inference costs compared to process-based models (de Burgh-Day & Leeuwenburg, 2023). For instance, once developed, these models tend to be less resource-intensive, offering a more efficient solution. Recent studies by Zhao et al. (2021) and Zheng et al. (2021) have demonstrated that data-driven modeling merely based on atmospheric forcing data can effectively emulate urban climates by modeling each computational grid cell independently with its own distinct model. However, such location-dependent emulators are less scalable and overlook geospatial data such as the urban surface parameters that can improve the emulation performance. Therefore, constructing a unified global model can be beneficial for easier application and communication, and it can also leverage global datasets to create a more accurate emulator. The unified emulator structure closely mirrors the fidelity of the process-based urban climate models, which are also unified (all grid cells share the same physical equations within the process-based models). Given that the model is largely nonlinear, machine learning (ML) can be applied to learn the nonlinearity between inputs and outputs (Irrgang et al., 2021; Mansfield et al., 2023).

ML modeling involves multiple steps, including feature engineering (encoding the input variables), model selection (choosing the machine learning algorithms) and hyperparameter optimization (optimizing the configuration of machine learning algorithms). Especially, model selection and hyperparameter optimization require substantial computational resources and expertise, making them challenging tasks for those unfamiliar with ML. Recently, automated machine learning (AutoML) frameworks have emerged, automatically recommending the “most suitable” ML algorithms and hyperparameter configurations for a given task to users (Thornton et al., 2013;

C. Wang et al., 2021). These frameworks are cost-effective (C. Wang et al., 2021) and have been successfully applied in environmental modeling studies (Wasala et al., 2024; Xia et al., 2023; Zheng et al., 2023). These frameworks enable scientists to streamline the complex model construction process, thereby accelerating the progress of research.

Therefore, this study aims to develop an AutoML-based approach to emulate a unified model of the global urban climate derived from process-based urban climate modeling. This approach is demonstrated with open data from CESM-LE as an example and can be extended to other process-based models when simulation data are available. We have also interpreted the ML models by developing a unified ranking score framework tailored for the AutoML tasks. In particular, we assessed the relative importance of atmospheric forcing, location and urban surface parameters to understand their contribution to emulating urban climates. These methods aid in building urban climate emulators to accelerate their practical application.

2 Methods

The overall workflow includes data processing, AutoML-based urban climate emulator development, and feature importance analysis (Figure 1). Data processing is detailed in Section 2.1, urban climate emulator development and experimental design are described in Section 2.2 and Section 2.3, and feature importance analysis framework is presented in Section 2.4.

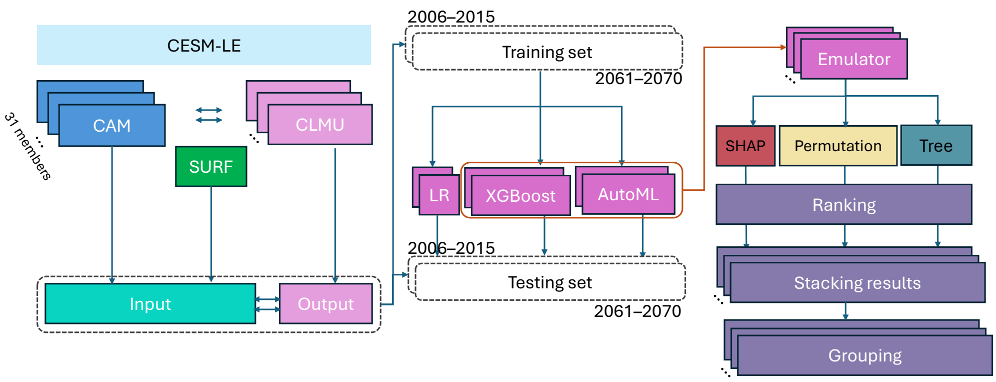

Fig. 1 Overview of the workflow. CAM is the atmospheric forcing from the atmospheric model in CESM; SURF is the urban surface parameters used in CESM-LE simulations; CLMU is the urban climate model in CESM, in this study; LR is the linear regression. The terms "SHAP", "permutation", and "tree" are three methods for feature importance evaluation (detailed in Section 2.4).

2.1 Urban climate model and data

We sourced our emulation data from the CESM-LE project, which provides ensemble simulation data derived from the Community Earth System Model (CESM). The

CESM is an open-source community model, with coupled atmosphere, ocean, land, river run-off, land-ice, and sea-ice components, which can simulate Earth's past, present and future climates (Danabasoglu et al., 2020). The Community Land Model Urban (CLMU) is an urban climate model and an important component of CESM's land model (K. Oleson et al., 2010), recognized as a valuable tool for urban climate studies (Sun et al., 2024; Zhao et al., 2021; Zheng et al., 2021). The detailed technical description of CLMU can be found in K. Oleson et al. (2010). In brief, CLMU models the urban areas as an "urban canyon". The structure of the urban canyon includes "urban columns", which comprise the roof, sunlit wall, shaded wall, impervious road and pervious road. The roads are centrally positioned within the canyon, flanked by building walls and roofs on both sides. Each component within these urban columns is parameterized with the morphological, radiative, and thermal properties, so that the energy balance and the related climate variables of urban areas can be calculated. It should be noted that in the current version of the CLMU, vegetation is not considered. Instead, a pervious canyon floor is used to approximate evaporation from vegetated surfaces.

Each member of CESM-LE runs at approximately 1° horizontal resolution in all model components for the period 1920-2100 (https://www.cesm.ucar.edu/community-projects/lens) (Kay et al., 2015), and is subjected to the same radiative forcing scenario but from a slightly different initial atmospheric state (created by randomly perturbing temperatures at the level of round-off error with an order of 10^{-14} K). The slight difference in the initial conditional will induce large differences in the internal variability (natural variability of the climate system resulting from nonlinear dynamical processes intrinsic to the atmosphere) (Zheng et al., 2021). In each CESM-LE member, variables from Community Atmosphere Model version 5 (CAM5) drive CLMU to produce the urban-related variables. In this study, we used the simulation data under a very high baseline emission scenario (Representative Concentration Pathways, RCP8.5 scenario) from CESM-LE, which is the highest greenhouse gas emissions scenario in the absence of climate change policies (Riahi et al., 2011). We extracted CLMU's daily maximum canyon air temperature (TREFMXAV_U in CLM history variable) as the label (or target for prediction) and the related CAM forcing as the features (or predictive variables) from 31 selected members (member 003–033) of CESM-LE with two time periods (2006–2015 and 2061–2070). The grid cells with urban areas in this study are presented in Figure S1. The urban surface parameters from the CESM-LE surface dataset were also used as features in our emulators (the distribution of each parameter is shown in Figure S2). The urban surface parameters originated from the global urban extent and urban properties developed by Jackson et al. (2010) while the building interior minimum and maximum temperatures were prescribed based on climate and socioeconomic considerations (K. Oleson et al., 2010). The urban extent was derived from LandScan 2004, a population density dataset derived from census data, nighttime lights satellite observations, road proximity, and slope (K. Oleson et al., 2010). Notably, the urban surface parameters and extent remained static in the simulations of CESM-LE, which means the urban surface parameters and urban fraction did not change over time. Due to the availability of global data, there are only 33 distinct regions defined by the urban surface data across the globe and the urban surface parameters in each region are assumed to be identical (K. Oleson et al., 2010).

2.2 Global urban daily temperature emulators

We built emulators to predict the daily maximum canyon air temperature to the framework described in Zhao et al. (2021) and Zheng et al. (2021). To assess how effectively geospatial data (location and urban surface parameters) contribute to the unified model of global urban climate, we developed and evaluated four types of emulators, as demonstrated in Eq. 1. Instead of constructing location-dependent emulators, we embedded the location and/or urban surface parameters into the input features or omitted them. This approach allowed us to consolidate the location-dependent models into a unified model for urban climate emulation. The four types of the emulators can be expressed as:

$$
\begin{aligned}
T &= f_1(\mathbf{AF}) \\
T &= f_2(\mathbf{AF}, \mathrm{LOC}) \\
T &= f_3(\mathbf{AF}, \mathrm{SURF}) \\
T &= f_4(\mathbf{AF}, \mathrm{LOC}, \mathrm{SURF}),
\end{aligned}
\tag{1}
$$

where T represents the daily maximum canyon air temperature, and $\mathbf{AF}$ denotes the vectors of atmospheric forcings. The $\mathbf{AF}$ includes net shortwave radiation, net longwave radiation and precipitation (liquid and solid) at the surface, and atmospheric temperature, pressure, specific humidity, and wind speed (zonal and meridional) at the forcing height, in total eight features. The LOC indicates the longitude and latitude of urban grid cells, while SURF refers to urban surface parameters, which are categorized into three types: morphological, radiative, and thermal parameters (detailed in Table 1). It is important to note that LOC and SURF are static over time, whereas T and $\mathbf{AF}$ vary along the time dimension. In this study, we did not include the time information (e.g., the month of the year) as features in our model, because the equations of the physical process do not vary monthly or daily. Details of emulator features are presented in Table 1.

The f_i represents different machine learning models with specific feature combinations. The best-performing emulator among these were selected for further analysis. We used multiple linear regression (LR) as the baseline to evaluate the linearity between features and the label. The standardization of all input features was applied for a robust result. Given that XGBoost–a scalable end-to-end tree boosting system (Chen & Guestrin, 2016)–has been successfully applied for the location-dependent urban climate emulation (Zheng et al., 2021), it is also included for comparison. For AutoML tasks, we employed the FLAML, a lightweight Python library for AutoML supporting fast and economical automatic tuning (C. Wang et al., 2021). This library chooses a search order optimized for both computational cost and model error and selects the models, hyperparameters, sample size and resampling strategy iteratively. FLAML has demonstrated a remarkable performance that outpaces other leading AutoML libraries (C. Wang et al., 2021). This tool has been proven to be useful for atmospheric and environmental research (Xia et al., 2023; Zheng et al., 2023). Specifically,

Table 1 Global daily maximum canyon air temperature emulator features

Category	Features	Full name	Unit
Atmospheric forcings	FLNS	Net longwave flux at surface	W/m^2
Atmospheric forcings	FSNS	Net solar flux at surface	W/m^2
Atmospheric forcings	PRECT	Total (convective and large-scale) precipitation rate (liquid + ice)	m/s
Atmospheric forcings	PRSN	Combination of large-scale (stable) snow rate (water equivalent) and convective snow rate (water equivalent)	m/s
Atmospheric forcings	QBOT	Lowest model level water vapor mixing ratio	kg/kg
Atmospheric forcings	TREFHT	Reference height temperature	K
Atmospheric forcings	UBOT	Lowest model level zonal wind	m/s
Atmospheric forcings	VBOT	Lowest model level meridional wind	m/s
Location	LAT	Latitude	Degree
Location	LON	Longitude	Degree
Morphological	CANYON_HWR	Canyon height to width ratio	Unitless
Morphological	HT_ROOF	Height of roof	meters
Morphological	THICK_WALL	Thickness of wall	meters
Morphological	WTLUNIT_ROOF	Fraction of roof	Unitless
Morphological	WTROAD_PERV	Fraction of pervious road	Unitless
Morphological	PCT_URBAN	Fraction of urban	Unitless
Radiative	EM_IMPROAD	Emissivity of impervious road	Unitless
Radiative	EM_PERROAD	Emissivity of pervious road	Unitless
Radiative	EM_ROOF	Emissivity of roof	Unitless
Radiative	EM_WALL	Emissivity of wall	Unitless
Radiative	ALB_IMPROAD	Albedo of impervious road	Unitless
Radiative	ALB_PERROAD	Albedo of pervious road	Unitless
Radiative	ALB_ROOF	Albedo of roof	Unitless
Radiative	ALB_WALL	Albedo of wall	Unitless
Thermal	T_BUILDING_MAX	Maximum interior building temperature	K
Thermal	T_BUILDING_MIN	Minimum interior building temperature	K
Thermal	TK_ROOF	Thermal conductivity of roof	W/m*K
Thermal	TK_WALL	Thermal conductivity of wall	W/m*K
Thermal	CV_ROOF	Volumetric heat capacity of roof	J/m^3*K
Thermal	CV_WALL	Volumetric heat capacity of wall	J/m^3*K
Thermal	TK_IMPROAD_0	Thermal conductivity of impervious road of urban layer 0	W/m*K
Thermal	CV_IMPROAD_0	Volumetric heat capacity of impervious road urban layer 0	J/m^3*K
Thermal	TK_IMPROAD_1	Thermal conductivity of impervious road of urban layer 1	W/m*K
Thermal	CV_IMPROAD_1	Thermal conductivity of impervious road of urban layer 1	J/m^3*K
Thermal	NLEV_IMPROAD	Number of impervious road layers	Unitless

three tree-based models were chosen for FLAML model selection process, including the Random Forests (RF) (Breiman, 2001), XGBoost, and LightBGM (a highly efficient gradient boosting decision tree) (Ke et al., 2017). The hyperparameters of these models were tuned using the default scheme of FLAML, which employed a root mean square error (RMSE) criterion and allocated a time budget of 21600 seconds (6 hours). Hyperparameter optimization was performed on the U.S. NSF NCAR Cheyenne high-performance computer using a 36-CPU compute node. Furthermore, the XGBoost models were also tuned by FLAML (but with XGBoost as the sole learner).

2.3 Experimental design

The experimental design is detailed in Figure 2 and Table 2. First, we built models as described in Section 2.2. The design encompasses four types of emulators, two sets of training data (2006–2015 and 2061–2070), and three algorithms for emulation tasks, resulting in a total of 24 modeling tasks. Specifically, four emulation schemes (Eq. 1) are CAM only, CAM+LOC, CAM+SURF and CAM+LOC+SURF. For the modeling tasks, the data were split into two groups, training data and testing data, for building and testing the emulators, respectively. Training data were randomly sampled at a rate of 3.33% from each member, with each selection using a different random state, which ensured that all the selected members were represented in the training set. Approximately 16.7 million samples were included in each training set. The distributions of the sampled atmospheric forcings and urban surface parameters in the training data are illustrated in Figure S3 and Figure S4, respectively. Data not sampled were used for testing purposes.

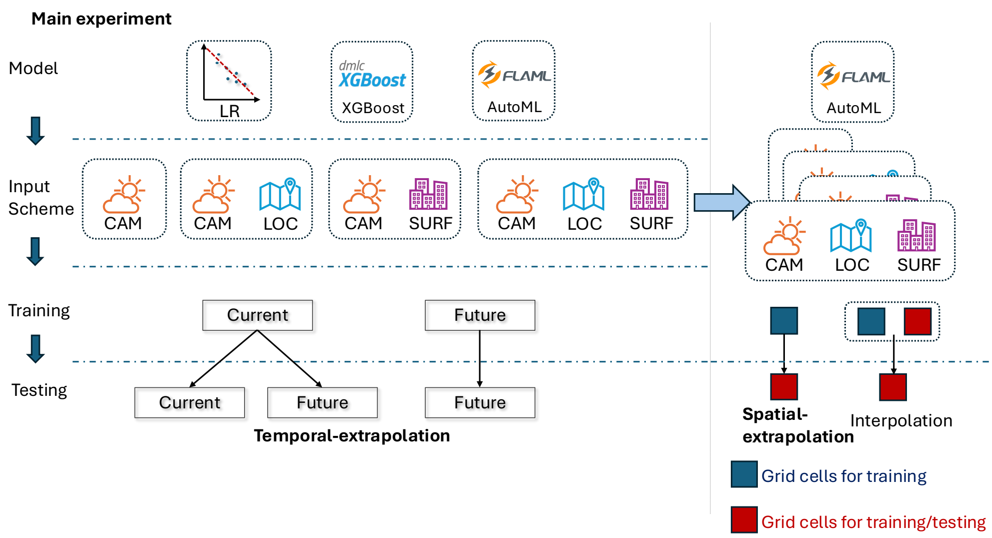

Fig. 2 Experimental design.

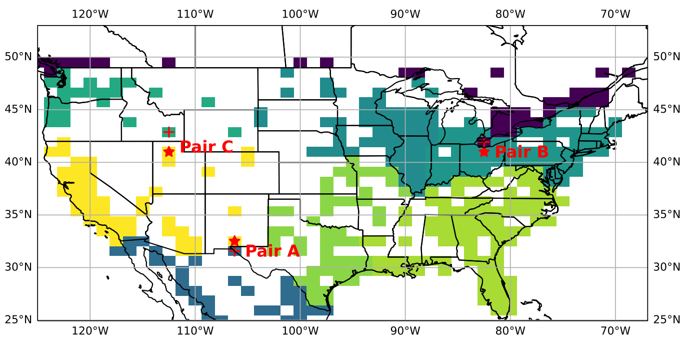

Fig. 3 Three selected grid cells and their neighbors. The symbol "+" indicates the selected grids for testing and "*" indicates the neighbors. Different colors indicate different grid cell IDs of 33 regions in CESM-LE urban surface dataset. Each region represents a different urban surface parameters group.

Model extrapolation is often necessary when making predictions for unseen input variable space. To test how well the data-driven model can emulate the global urban climate, we explored the extrapolations of models in two ways. (1) We examined the temporal extrapolation performance by training the models with the 2006–2015 dataset and testing the models with the 2061–2070 dataset. The datasets used in this study are under the RCP8.5 scenario, indicating significant changes in climate variables due to global warming over a span of fifty years. They include 31 members, each representing various climate conditions affected by internal climate variability (Deser et al., 2012). This allows us to test whether the models are well-generalized for future climate change. (2) Given that urban surface parameters vary across the 33 regions (K. Oleson et al., 2010), we also assessed the spatial extrapolation performance of the models across the different regions. This assessment used three pairs of urban grid cells from the dataset. Each pair consists of neighboring grid cells located in different regions but are close in space (Figure 3), reflecting disparities in urban surface parameters and similarity in location. These three pairs were then separated for training and testing, respectively. To test the spatial extrapolation performance, we extracted the data containing the testing grid cell from 2061–2070 of CESM-LE, SEtest (113150 samples), then we tested the unified global models' performance trained by the dataset including all urban grid cells using SEtest (34–37 in Table 2). This serves as interpolation baselines for the spatial extrapolation assessment, which represents no spatial extrapolation as a control group. We also extracted the data containing the training grid cell from the training set and the testing grid cell from the training set, respectively, which were named SEtrain (3000 samples) and SEitrain (3000 samples), to train the models. Global models trained by the dataset excluding SEtrain were evaluated by the same testing set (38–41 in Table 2) to test the spatial extrapolation. To further explain the spatial extrapolation of the global model, we also trained models by SEtrain and SEitrain, respectively (42–44 in Table 2). All experiments in this section were trained and tested using the dataset range from 2061–2070. The details on spatial extrapolation experiments can be found in Table 2.

Table 2 Experimental design. The time periods "2016–2015" and "2061–2070" represent the data set ranges from CESM-LE.

ID	Method	Input features	Training data	Testing set data
model selection and evaluation				
1	FLAML	CAM	2006–2015	2006–2015
2	FLAML	CAM LOC	2006–2015	2006–2015
3	FLAML	CAM SURF	2006–2015	2006–2015
4	FLAML	CAM LOC SURF	2006–2015	2006–2015
5	FLAML	CAM	2061–2070	2061–2070
6	FLAML	CAM LOC	2061–2070	2061–2070
7	FLAML	CAM SURF	2061–2070	2061–2070
8	FLAML	CAM LOC SURF	2061–2070	2061–2070
9	XGBoost	CAM	2006–2015	2006–2015
10	XGBoost	CAM LOC	2006–2015	2006–2015
11	XGBoost	CAM SURF	2006–2015	2006–2015
12	XGBoost	CAM LOC SURF	2006–2015	2006–2015
13	XGBoost	CAM	2061–2070	2061–2070
14	XGBoost	CAM LOC	2061–2070	2061–2070
15	XGBoost	CAM SURF	2061–2070	2061–2070
16	XGBoost	CAM LOC SURF	2061–2070	2061–2070
17	LR	CAM	2006–2015	2006–2015
18	LR	CAM LOC	2006–2015	2006–2015
19	LR	CAM SURF	2006–2015	2006–2015
20	LR	CAM LOC SURF	2006–2015	2006–2015
21	LR	CAM	2061–2070	2061–2070
22	LR	CAM LOC	2061–2070	2061–2070
23	LR	CAM SURF	2061–2070	2061–2070
24	LR	CAM LOC SURF	2061–2070	2061–2070
temporal extrapolation				
25	FLAML	CAM	2006–2015	2061–2070
26	FLAML	CAM LOC	2006–2015	2061–2070
27	FLAML	CAM LOC SURF	2006–2015	2061–2070
28	XGBoost	CAM	2006–2015	2061–2070
29	XGBoost	CAM LOC	2006–2015	2061–2070
30	XGBoost	CAM LOC SURF	2006–2015	2061–2070
31	LR	CAM	2006–2015	2061–2070
32	LR	CAM LOC	2006–2015	2061–2070
33	LR	CAM LOC SURF	2006–2015	2061–2070
spatial extrapolation				
34	FLAML	CAM	2061–2070	SEtest
35	FLAML	CAM LOC	2061–2070	SEtest
36	FLAML	CAM SURF	2061–2070	SEtest
37	FLAML	CAM LOC SURF	2061–2070	SEtest
38	FLAML	CAM	2061–2070 exclude SEtrain	SEtest
39	FLAML	CAM LOC	2061–2070 exclude SEtrain	SEtest
40	FLAML	CAM SURF	2061–2070 exclude SEtrain	SEtest
41	FLAML	CAM LOC SURF	2061–2070 exclude SEtrain	SEtest
42	FLAML	CAM	SEtrain	SEtest
43	FLAML	CAM	SEitrain	SEtest

2.4 Feature importance evaluation

To evaluate the feature importance, Schreck et al. (2023) applied the feature importance derived from tree-based model, permutation feature importance, and SHapley Additive exPlanations (SHAP) methods to help interpret predictors based on input. Meanwhile, Zheng et al. (2023) proposed a ranking source method that unified different feature importance results derided from tree-based model. Inspired by these approaches, here we developed a unified ranking score framework tailored for the AutoML tasks, combining tree-based feature importance, permutation feature importance, and SHAP values, to evaluate the relative importance of different features (Schreck et al., 2023; Zheng et al., 2023). This "ensemble method" improves the robustness of our analysis by not relying solely on a single type of feature importance evaluation.

Tree-based models are developed by node split that is based on features, which allows us to export the feature importance directly by calculating the number of feature splits in the tree, feature split gain, or coverage of feature splits. In this study, the ML models are all typical tree-based models, and thus we derived the feature importance from the model directly (named the tree-based method in this study). Notably, the feature importance in RF is calculated using the Gini importance by default, which measures the total (normalized) reduction in the criterion brought by each feature; In XGBoost and LightGBM, feature importance is determined by counting the number of times a feature is used to split the data across all trees by default.

For the permutation method, the feature importance is a general method applicable to all models fitted using tabular data. The permutation feature importance can be obtained by calculating the decrease in a model score when randomly shuffling a single feature value (Breiman, 2001). The calculation is as follows,

$$i_j = s - \frac{1}{K}\sum_{k=1}^{K} s_{k,j},$$

where i_j indicates the importance of feature j, s indicates the selected reference score of the model (e.g., RMSE in this study), $s_{k,j}$ indicates the score of k^{th} repetition for calculation of the feature j permutation importance. K is the number of repetitions for calculating permutation feature importance (30 in this study).

We also applied Shapley Additive exPlanations (SHAP), a model-agnostic representation of feature importance where the impact of each feature on the model is represented using Shapley values (Lundberg & Lee, 2017; Lundberg et al., 2018). The SHAP value is calculated based on the following,

$$\phi_i(f,x) = \sum_{S\subseteq S_{\mathrm{all}\setminus\{i\}}} \frac{|S|!\,(M-|S|-1)!}{M!}\left[f_x\left(S\cup\{i\}\right) - f_x\left(S\right)\right],$$

where $\phi_i(f,x)$ is the SHAP value of the prediction of model f for input x, $f(S)$ denotes the model's output given a specific feature subset S. The summation of all possible feature subsets S is calculated by each subset weighted according to its contribution to the model's output. The contribution is calculated as the difference in the model's output when feature i is added compared to when it is absent. We calculated the absolute of all mean SHAP values of the select inputs, allowing us to compare with the methods mentioned above.

It should be noted that employing the permutation and SHAP methods requires substantial computational resources and time. Given the considerable size of the datasets and the model in this study, it is impractical to use the entire training set to calculate permutation and SHAP importance directly. Therefore, we randomly extracted 1% samples from each grid cell in the training set (about 167,000 samples) to compute permutation feature importance and SHAP values.

The metrics of feature importance derived from the different above analysis methods are challenging to compare because they are based on different principles. Hence, we derived a "ranking score" metric to unify the comparison of feature importance from different methods (Zheng et al., 2023). For each interpretation method, the feature importance values were ranged in ascending order and assigned a "ranking score" to each feature based on its position in the ordered list of importance values. Specifically, the feature with the lowest importance was assigned a score of 1, the second least important feature was a score of 2, and so forth. Consequently, the ranking scores were constrained within the range from 1 (indicating the least important one) to the total number of features (representing the most important one). This normalization ensures that the feature importance scores from different methods are transformed onto a consistent scale. We also categorized features (Table 1) and calculated the mean ranking score within each feature type.

3 Results and discussion

3.1 AutoML and geospatial data improve the emulation performance

The FLAML, XGBoost and LR were employed to emulate the daily maximum canyon air temperature across two distinct periods, current (2006–2015) and future (2061–2070). The R-squared values of the testing set ranged between 0.97 to 0.99 (Figure S5). The lowest mean absolute error (MAE) is 0.57 K from the FLAML model (Figure S6). Here we focused on the the root mean squared error (RMSE), known for imposing heightened penalties on larger errors and demonstrating sensitivity to outliers. The RMSE of FLAML and XGBoost models is lower than the LR as they captured the complex nonlinear interactions within the CLMU, which LR can not well deal with (Figure 4). The FLAML model, with 0.81 K RMSE outperformed both XGBoost and LR (Figure 4), underlining the capability of AutoML to develop a more reliable and robust model for urban climatic dynamics. By applying FLAML, researchers can be rescued from model selection and hyperparameter optimization.

The addition of geospatial data (LOC and/or SURF) can improve the performance of the nonlinear ML models, but this is not the case with LR (Figure 4). This indicates the relationship between the input variables within LOC and SURF, and the output variable, is nonlinear, which LR cannot effectively capture. Therefore, even if more features are added, the improvement in LR's performance remains marginal, underscoring the importance of choosing the right model. It is interesting to note that LOC is more beneficial for constructing the global urban climate data-driven model, as LOC leads to a greater reduction in the model's RMSE compared to SURF (Figure 4). It is reasonable that the LOC should provide more information, for example, when a location is fixed, the urban surface parameters and some geographical properties of this location should be fixed, indicating the SURF potentially depends on the LOC (can be expressed as SURF $= g(\mathrm{LOC})$). In addition, within the surface dataset used in CLMU, lots of urban areas possess similar urban parameters even with different LOC, in other words, SURF does not possess enough information as provided by LOC. Geographical location can provide a proxy for additional determinants of temperature differences beyond surface cover parameters, such as background climate. Indeed, in some cases the influence of these determinants may be greater than urban effects due to surface properties. Consequently, ML models parameterized with LOC yield superior performance than those with SURF.

Models parameterized with LOC and SURF can further increase the performance of ML models, though the improvement is relatively minor (Figure 4). This demonstrates that the ML models do not fully capture the LOC information, and coupling the LOC and SURF can help the ML models understand the connection between location and the local urban surface parameters, thereby improving model performance. The complexity arises when approximating $T = f(AF, \mathrm{LOC}) \rightleftharpoons f^{'}(AF, \mathrm{LOC}, g(\mathrm{LOC}))$ compared to directly approximating $T = f(AF, \mathrm{LOC}, \mathrm{SURF})$, because of the additional function g. Another possible reason is that the "LOC + SURF" scheme provides more information that the data-driven model can learn from to extract the complex relationship behind the process-based models. Generally, constructing an ML emulator with more detailed data from process-based models would be beneficial, though this is not universally the case. Although the integration of geographical location and urban surface parameters yields only a slight improvement (<1 K) in the urban emulator's performance, this modest increment is important in urban climate modeling.

3.2 The global emulator is well extrapolated temporally

A large amount of data has been used as testing data for model evaluation to thoroughly evaluate the robustness of the urban temperature emulator. Despite this, the application of the emulator may still encounter two types of extrapolation challenges: temporal extrapolation (CAM forcings are different) and spatial extrapolation (the emulator is applied to an unseen location by the training data). To test the generalization of the emulators, we explored these two types of extrapolation.

We tested the models trained on data from 2006–2015 using future data spanning 2061–2070. Notably, the CESM-LE simulations lacked scenarios involving a developing urban surface under RCP8.5, resulting in a static urban representation (Jones et al., 2018; K.W. Oleson et al., 2018). Thus, changes in future urban temperature are primarily affected by atmospheric forcing due to greenhouse gas-induced global warming. The findings reveal that ML models excel in extrapolating atmospheric forcing changes, particularly the FLAML model with "LOC+SURF", as indicated by lower RMSE values (Figure 5). This underscores the utility of the "LOC+SURF" scheme in facilitating extrapolation.

In further exploration, we investigated the impact of geographical variations on the emulator performance. The three selected grid cell pairs for exploration testing are

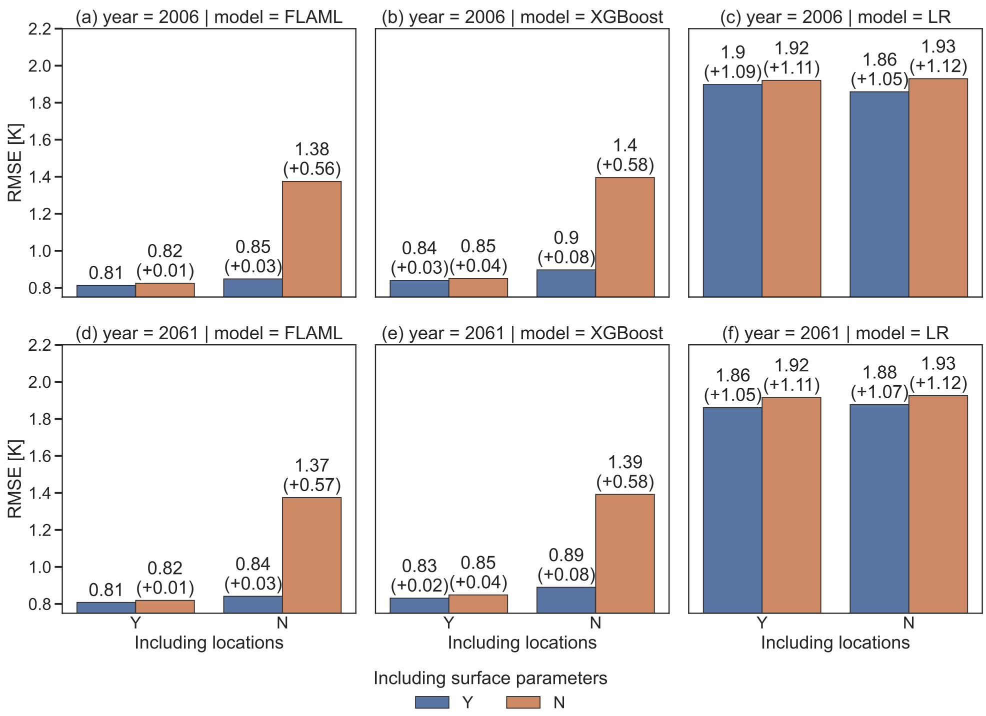

Fig. 4 RMSE of different models and their differences compared to baseline. (a), (b) and (c) indicate the training set ranges from 2006–2015; (d), (e) and (f) indicate the training set ranges from 2061–2070; (a) and (d) indicate modeling by FLAML; (b) and (e) indicate modeling by XGBoost; (c) and (f) indicate modeling by LR; Y indicates Yes (i.e., with LOC/SURF), N indicates No (i.e., without LOC/SURF). Bar labels within the parenthesis of (a), (b), and (c) use the first column of (a) as the baseline. Bar labels within the parenthesis of (d), (e), and (f) use the first column of (d) as the baseline.

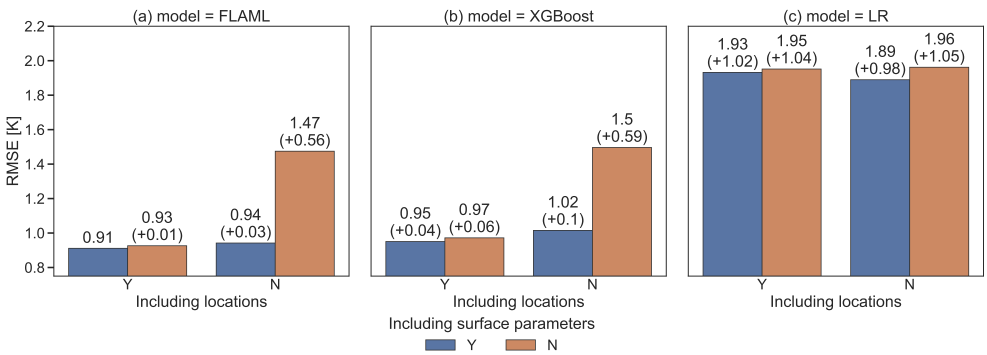

Fig. 5 RMSE of different models for temporal extrapolation and their differences compared to baseline. (a) indicates modeling by FLAML; (b) indicates modeling by XGBoost; (c) indicates modeling by LR; Y indicates YES (i.e., with LOC/SURF), N indicates NO (i.e., without LOC/SURF). Bar labels within the parenthesis of (a), (b), and (c) use the first column of (a) as the baseline.

depicted in Figure 3. We used the global training data not including the selected grid cells to train a global urban temperature emulator and tested with the selected grid cells (SEtest in Section 2.3). Our findings indicated that the emulator incorporating LOC exhibited superior performance, whereas the schemes of "LOC+SURF" did not consistently yield better results. Moreover, our results revealed that the utilization of SURF not only failed to enhance extrapolation but even led to an increase in RMSE (Figure 6). This suggests potential inaccuracies in the global emulator incorporating urban surface parameters when extrapolating geographical locations.

It is expected that neighboring grid cells share similar latitude, longitude and other geographical properties, thus suggesting the potential for relatively good extrapolation performance. We built the neighbor emulators (orange of Figure 6) of the selected neighborhood grid cells (SEtest in Section 2.3) and used the selected grid cells (SEtest in Section 2.3) to test the spatial exploration performance. The result shows that neighbor models can not well predict the temperature of the neighbor grid cells, that is, neighbor models inadequately emulate the urban climate process of their neighbors (Figure 6). This inadequacy may stem from subtle differences in urban geographical positions and surface properties, which may be important for urban climate emulator performance. Additionally, the performance of neighbor models surpassed that of the global model lacking LOC and SURF parameters but worse than the global model solely parameterized with LOC (Figure 6), signifying the benefits of global models in predictive capabilities.

Lastly, we evaluated the model interpolation, which involves two types. The first type is the interpolation of a global model where the model was trained by the global training set and tested by the SEtest (red of Figure 6). The other interpolation experiment is that trained the model by SEitrain and tested the model by SEtest (green of Figure 6). All global models, except those without LOC and SURF features, exhibited satisfactory performance. Notably, models that incorporated LOC and SURF features demonstrated the best results (Figure 6). Moreover, the global models that incorporate LOC and/or SURF features outperformed those trained by only one grid cell, suggesting that global models provide more accurate predictions than location-dependent models. This improvement may be attributed to the advantages of using large datasets in data-driven models. In summary, our results indicate that a global emulator can be well extrapolated at spatial dimensions and is more efficient in emulating urban climate than the location-dependent model.

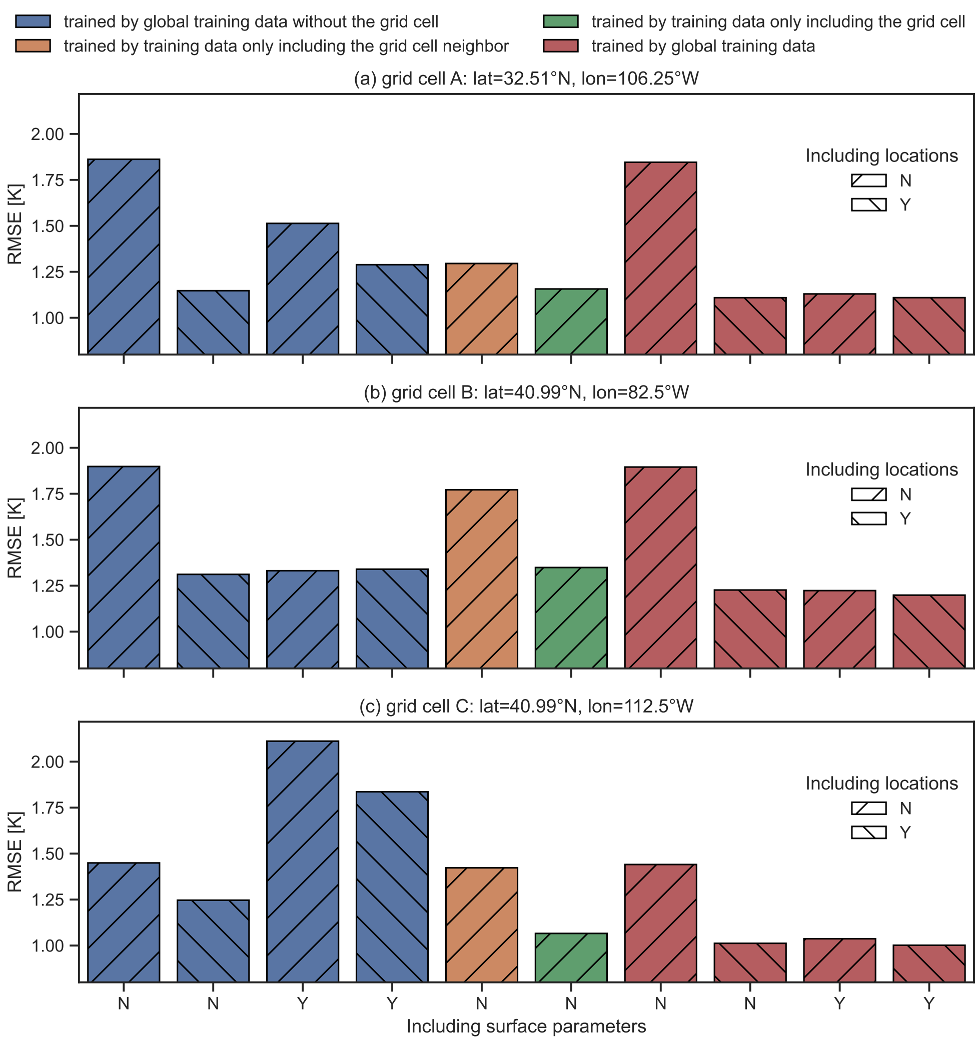

Fig. 6 RMSE of different FLAML models for spatial extrapolation. (a), (b) and (c) indicate three selected grid cells respectively; Y indicates YES (i.e., with LOC/SURF), N indicates NO (i.e., without LOC/SURF).

3.3 Morphological parameters are more important than radiative and thermal parameters

We employed three methods to interpret emulators, including tree-based feature importance, permutation feature importance, and SHAP values. Due to their distinct underlying principles, these methods often produce feature importance values that vary not only in magnitude but also in scale (Schreck et al., 2023). For example, some methods generate values ranging from 0 to 1, while others may produce values from

0 to 10,000. This variance in scale makes direct comparisons between methods unreasonable. To address this, we normalized the results using "ranking scores" (details in Section 2.4), allowing us to different methods and amalgamate outcomes from different methods into a unified, comparable result. This framework enhances the applicability of AutoML in feature importance analysis.

A consistent trend in variable ranking scores predominantly follows the order of CAM/LOC > SURF (Figure 7 and Figure S7-12). This trend suggests that within the model, the importance of SURF is inferior to that of LOC, reinforcing our earlier findings in Section 3.1. This is a reasonable result because the CAM forcing and location determine the basis of background climate while the SURF affects the background climate on a relatively small spatial scale. However, the SURF is critical for emulating the local urban climate because, although the difference between the local urban climate and the background climate is small relative to the overall background climate, this small difference can heavily influence the urban environment. For the importance of different categories within SURF, urban morphology variables (MOR) held the highest ranking scores (Figure 7). In other words, urban morphology is sensitive to urban maximum temperature emulation.

Discrepancies are presented in the ranking of RAD and THM between the FLAML and XGBoost models. In XGBoost, RAD scored higher on average than THM, while FLAML presented RAD $\approx$ THM. The approaches of feature importance exploring inherently rely on establishing precise models. For instance, lower model accuracy signifies potential errors in the tree structure parameters, and the computation for permutation importance and SHAP also require well-trained models. Therefore, in this study, results derived from FLAML models are more trusted as they get better performance (Figure 4 and Figure 5).

It is noteworthy that the results from the tree-based models align in the order of CAM > LOC > MOR > RAD > THM, while permutation and SHAP show CAM $\approx$ LOC > MOR > RAD $\approx$ THM (Figure S12 and S14). These disparities among different feature importance methods were partially eliminated by combining them. Thus, we recommend that the unified result (CAM > LOC > MOR > RAD $\approx$ THM).

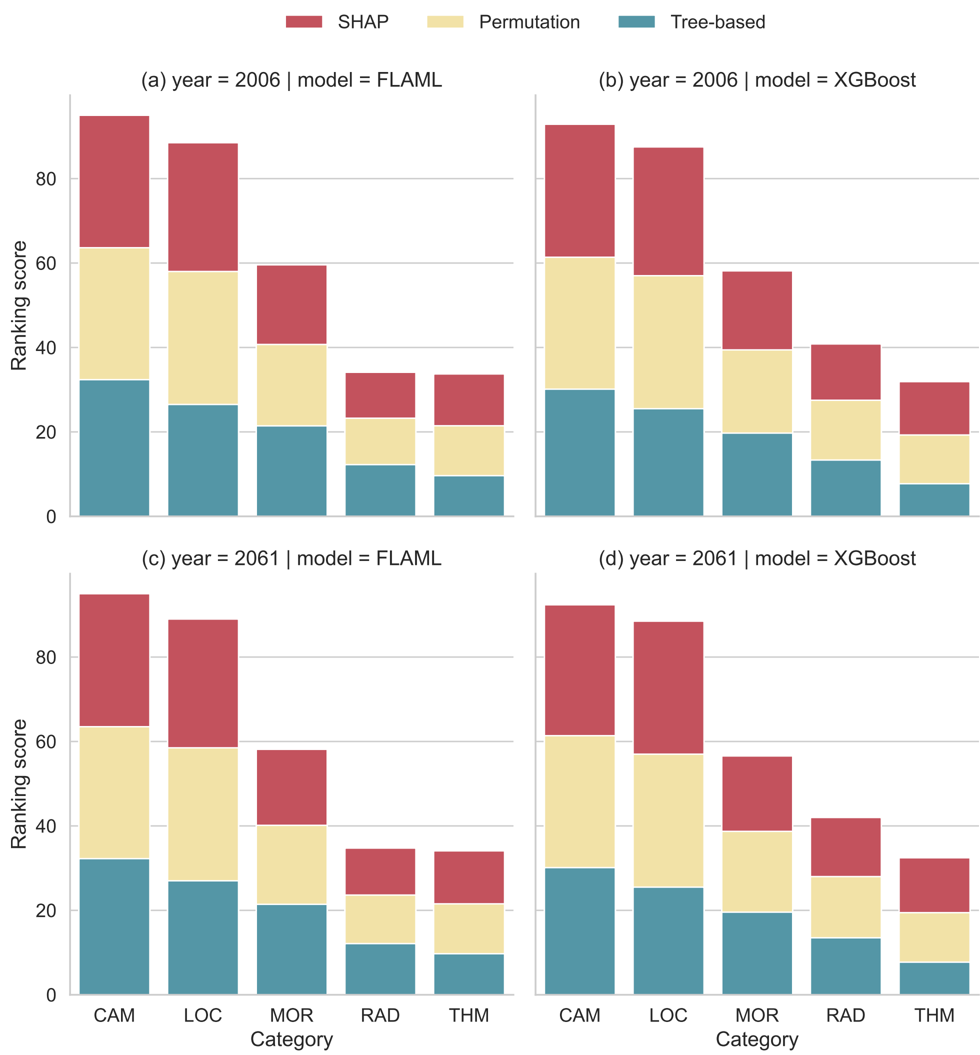

Fig. 7 Average ranking score in different categories of different models using tree-based, permutation and SHAP methods. (a) and (b) indicate the training set ranges from 2006–2015; (c) and (d) indicate the training set ranges from 2061–2070; (a) and (c) indicate modeling by FLAML; (b) and (d) indicate modeling by XGBoost; CAM indicates atmospheric forcing from CAM; LOC indicates locations; MOR, RAD and THM indicates morphological, radiative and thermal urban surface parameters, respectively

The importance of each input feature was also evaluated. The result reveals that the importance of LOC is on par with some CAM variables (Figure 8), possibly due to LOC being co-linear with some forcing variables, such as the solar radiation. Moreover, our analysis identified PCT_URBAN (morphological), CANYON_HWR (morphological) and ALB_WALL (radiative) as the top three important urban surface parameters among all models (Figure 8). This underscores their critical contribution to accurately emulating urban temperatures. We also observed shifts in the importance of urban surface parameters between models trained on current versus future data. Notably, the significance of THICK_ROOF (morphological), ranking fourth in 2006–2015, demonstrated a decrease in importance in 2061–2070. These evolving trends highlight the differential roles that current and future urban variables play in emulating urban climates.

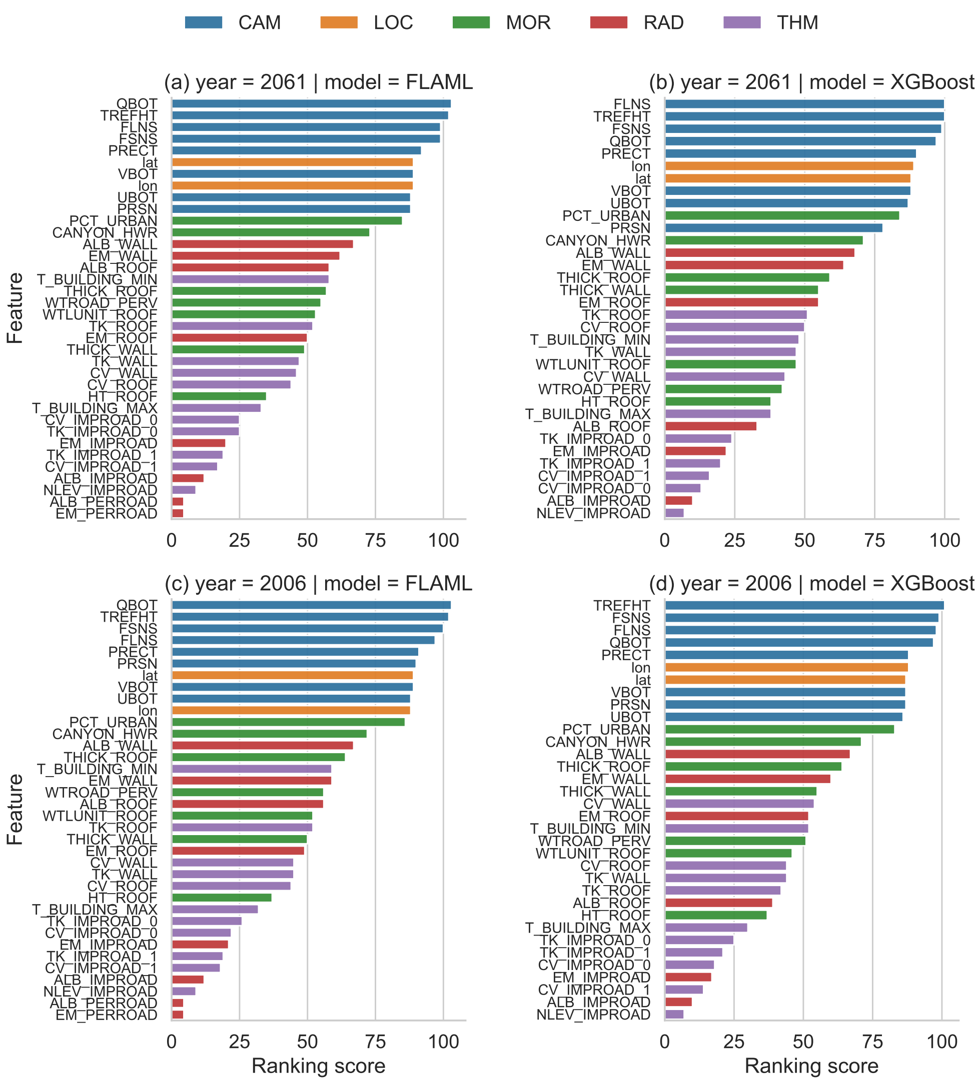

Fig. 8 Total Ranking score of tree-based, permutation and SHAP methods in different models. (a) and (b) indicate the training set ranges from 2006–2015; (c) and (d) indicate the training set ranges from 2061–2070; (a) and (c) indicate modeling by FLAML; (b) and (d) indicate modeling by XGBoost; CAM indicates atmospheric forcing from CAM; LOC indicates locations; MOR, RAD and THM indicates morphological, radiative and thermal urban surface parameters, respectively

4 Conclusions

The purpose of this study is to develop an AutoML-based approach for efficiently emulating the unified global urban climate, promoting the urban climate model application. As a demonstration, we built the unified global urban daily maximum 2-m temperature emulators of CLMU using the open-source CESM-LE data. We also designed experiments to probe how the location and urban surface parameters can aid in building an urban climate emulator. To understand the feature importance for emulating, a unified ranking score framework integrating importance derived from the tree-based model, permutation and SHAP, was applied to interpret the AutoML models.

The efficiency of AutoML-based method is well-generalized for building the unified global urban climate emulators. By providing geographical features–location and surface parameters, the emulators can learn the dynamics of urban climate well. The emulators were further tested by temporal and spatial extrapolation and showed the robust adaptability of AutoML model to predict urban temperature under climate change, which benefits from the unified global emulator. However, the emulator can not well extrapolate on the spatial dimension. Thus, we suggest training the emulator that includes all the locations, e.g., a global emulator, to prevent spatial extrapolation.

The ranking score results indicate that forcing variables and location are the most important in emulating the urban climate model followed by urban surface parameters. Among the surface parameters, urban morphological parameters markedly contribute to the urban daily maximum 2-m temperature emulators.

Although urban areas occupy a relatively small portion of the landscape, they significantly contribute to climate alteration with land surface modifications and anthropogenic emissions. This urban climate dynamic is currently underrepresented in some Earth system models. AutoML is a promising solution to emulate these processes effectively. Employing AutoML to develop data-driven urban climate models can streamline their application, mitigating the complexities of model environment configuration and installation, and reducing high computational costs. Emulation via AutoML can also rapidly estimate urban climate based on multiple multi-urban model ensembles without running the urban climate models that require their own specific environment configuration, thereby enhancing the application and precision of urban climate models. Consequently, the integration of AutoML can potentially advance the field of urban climate modeling with myriad opportunities for evaluating adaptation strategies.

Acknowledgments. This material is based upon work supported by the U.S. NSF National Center for Atmospheric Research, which is a major facility sponsored by the U.S. National Science Foundation under Cooperative Agreement No. 1852977. We would like to acknowledge high-performance computing support from Cheyenne and Casper provided by NSF NCAR's Computational and Information Systems Laboratory, sponsored by the National Science Foundation. We also thank Earth on AWS and Microsoft AI for Earth awards for providing cloud credits for research. ZZ acknowledges support from NSF NCAR Advanced Study Program Postdoctoral Fellowship. The authors declare no conflict of interest.

5 Code and data availability

Code to reproduce the emulations is available at https://github.com/envdes/code_UrbFLAML.

References

Baklanov, A., Grimmond, C., Carlson, D., Terblanche, D., Tang, X., Bouchet, V., ... Hovsepyan, A. (2018). From urban meteorology, climate and environment research to integrated city services. *Urban Climate*, *23*, 330–341, https://doi.org/10.1016/j.uclim.2017.05.004

Breiman, L. (2001). Random Forests. *Machine Learning*, *45*(1), 5–32, https://doi.org/10.1023/A:1010933404324

Chen, T., & Guestrin, C. (2016). XGBoost: A scalable tree boosting system. *Proceedings of the 22nd ACM SIGKDD international conference on knowledge discovery and data mining* (pp. 785–794). New York, NY, USA: Association for Computing Machinery.

Danabasoglu, G., Lamarque, J.-F., Bacmeister, J., Bailey, D.A., DuVivier, A.K., Edwards, J., ... Strand, W.G. (2020). The community earth system model version 2 (CESM2). *Journal of Advances in Modeling Earth Systems*, *12*(2), e2019MS001916, https://doi.org/10.1029/2019MS001916

de Burgh-Day, C.O., & Leeuwenburg, T. (2023). Machine learning for numerical weather and climate modelling: A review. *Geoscientific Model Development*, *16*(22), 6433–6477, https://doi.org/10.5194/gmd-16-6433-2023

Deser, C., Phillips, A., Bourdette, V., Teng, H. (2012). Uncertainty in climate change projections: The role of internal variability. *Climate Dynamics*, *38*(3), 527–546, https://doi.org/10.1007/s00382-010-0977-x

Dimoudi, A., Kantzioura, A., Zoras, S., Pallas, C., Kosmopoulos, P. (2013). Investigation of urban microclimate parameters in an urban center. *Energy and Buildings*, *64*, 1–9, https://doi.org/10.1016/j.enbuild.2013.04.014

Dottori, F., Szewczyk, W., Ciscar, J.-C., Zhao, F., Alfieri, L., Hirabayashi, Y., ... Feyen, L. (2018). Increased human and economic losses from river flooding with anthropogenic warming. *Nature Climate Change*, *8*(9), 781–786, https://doi.org/10.1038/s41558-018-0257-z

Gasper, R., Blohm, A., Ruth, M. (2011). Social and economic impacts of climate change on the urban environment. *Current Opinion in Environmental Sustainability*, *3*(3), 150–157, https://doi.org/10.1016/j.cosust.2010.12.009

Ghanbari, M., Arabi, M., Georgescu, M., Broadbent, A.M. (2023). The role of climate change and urban development on compound dry-hot extremes across US cities. *Nature Communications*, *14*(1), 3509, https://doi.org/10.1038/s41467-023-39205-x

Hu, J., He, G., Meng, R., Gong, W., Ren, Z., Shi, H., … Ma, W. (2023). Temperature-related mortality in China from specific injury. *Nature Communications*, *14*(1), 37, https://doi.org/10.1038/s41467-022-35462-4

Irrgang, C., Boers, N., Sonnewald, M., Barnes, E.A., Kadow, C., Staneva, J., Saynisch-Wagner, J. (2021). Towards neural Earth system modelling by integrating artificial intelligence in Earth system science. *Nature Machine Intelligence*, *3*(8), 667–674, https://doi.org/10.1038/s42256-021-00374-3

Jackson, T.L., Feddema, J.J., Oleson, K.W., Bonan, G.B., Bauer, J.T. (2010). Parameterization of Urban Characteristics for Global Climate Modeling. *Annals of the Association of American Geographers*, *100*(4), 848–865, https://doi.org/10.1080/00045608.2010.497328

Jones, B., Tebaldi, C., O'Neill, B.C., Oleson, K., Gao, J. (2018). Avoiding population exposure to heat-related extremes: Demographic change vs climate change. *Climatic Change*, *146*(3), 423–437, https://doi.org/10.1007/s10584-017-2133-7

Kay, J.E., Deser, C., Phillips, A., Mai, A., Hannay, C., Strand, G., … Vertenstein, M. (2015). The community earth system model (CESM) large ensemble project: A community resource for studying climate change in the presence of internal climate variability. *Bulletin of the American Meteorological Society*, *96*(8), 1333–1349, https://doi.org/10.1175/BAMS-D-13-00255.1

Ke, G., Meng, Q., Finley, T., Wang, T., Chen, W., Ma, W., … Liu, T.-Y. (2017). LightGBM: A highly efficient gradient boosting decision tree. *Proceedings of the 31st international conference on neural information processing systems* (pp. 3149–3157). Red Hook, NY, USA: Curran Associates Inc.

Liang, L., & Gong, P. (2020). Urban and air pollution: A multi-city study of long-term effects of urban landscape patterns on air quality trends. *Scientific Reports*, *10*(1), 18618, https://doi.org/10.1038/s41598-020-74524-9

Lipson, M.J., Grimmond, S., Best, M., Abramowitz, G., Coutts, A., Tapper, N., … Pitman, A.J. (2024). Evaluation of 30 urban land surface models in the Urban-PLUMBER project: Phase 1 results. *Quarterly Journal of the Royal Meteorological Society*, *150*(758), 126–169, https://doi.org/10.1002/qj.4589

Liu, H., Huang, B., Yang, C. (2020). Assessing the coordination between economic growth and urban climate change in China from 2000 to 2015. *Science of The Total Environment*, *732*, 139283, https://doi.org/10.1016/j.scitotenv.2020.139283

Lundberg, S.M., & Lee, S.-I. (2017). A unified approach to interpreting model predictions. *Proceedings of the 31st international conference on neural information processing systems* (pp. 4768–4777). Red Hook, NY, USA: Curran Associates Inc.

Lundberg, S.M., Nair, B., Vavilala, M.S., Horibe, M., Eisses, M.J., Adams, T., ... Lee, S.-I. (2018). Explainable machine-learning predictions for the prevention of hypoxaemia during surgery. *Nature Biomedical Engineering*, *2*(10), 749–760, https://doi.org/10.1038/s41551-018-0304-0

Mansfield, L.A., Gupta, A., Burnett, A.C., Green, B., Wilka, C., Sheshadri, A. (2023). Updates on model hierarchies for understanding and simulating the climate system: A focus on data-informed methods and climate change impacts. *Journal of Advances in Modeling Earth Systems*, *15*(10), e2023MS003715, https://doi.org/10.1029/2023MS003715

Oleson, K., Bonan, G., Feddema, J., Vertenstein, M., Kluzek, E. (2010). *Technical Description of an Urban Parameterization for the Community Land Model (CLMU)* (Tech. Rep.).

Oleson, K.W., Anderson, G.B., Jones, B., McGinnis, S.A., Sanderson, B. (2018). Avoided climate impacts of urban and rural heat and cold waves over the U.S. using large climate model ensembles for RCP8.5 and RCP4.5. *Climatic Change*, *146*(3), 377–392, https://doi.org/10.1007/s10584-015-1504-1

Potere, D., & Schneider, A. (2007). A critical look at representations of urban areas in global maps. *GeoJournal*, *69*(1), 55–80, https://doi.org/10.1007/s10708-007-9102-z

Qi, G., Che, J., Wang, Z. (2023). Differential effects of urbanization on air pollution: Evidences from six air pollutants in mainland China. *Ecological Indicators*, *146*, 109924, https://doi.org/10.1016/j.ecolind.2023.109924

Riahi, K., Rao, S., Krey, V., Cho, C., Chirkov, V., Fischer, G., ... Rafaj, P. (2011). RCP 8.5—A scenario of comparatively high greenhouse gas emissions. *Climatic Change*, *109*(1), 33, https://doi.org/10.1007/s10584-011-0149-y

Ritchie, H., Samborska, V., Roser, M. (2024). Urbanization. *Our World in Data*, ,

Romero-Lankao, P., Bulkeley, H., Pelling, M., Burch, S., Gordon, D.J., Gupta, J., ... Munshi, D. (2018). Urban transformative potential in a changing climate. *Nature Climate Change*, *8*(9), 754–756, https://doi.org/10.1038/s41558-018-0264-0

Schneider, A., Friedl, M.A., Potere, D. (2009). A new map of global urban extent from MODIS satellite data. *Environmental Research Letters*, *4*(4), 044003, https://doi.org/10.1088/1748-9326/4/4/044003

Schreck, J.S., Petzke, W., Jiménez, P.A., Brummet, T., Knievel, J.C., James, E., ... Gagne, D.J. (2023). Machine learning and VIIRS satellite retrievals for skillful fuel moisture content monitoring in wildfire management. *Remote Sensing*, *15*(3372), , https://doi.org/10.3390/rs15133372

Shahrestani, M., Yao, R., Luo, Z., Turkbeyler, E., Davies, H. (2015). A field study of urban microclimates in London. *Renewable Energy*, *73*, 3–9, https://doi.org/10.1016/j.renene.2014.05.061

Sun, Y., Fang, B., Oleson, K.W., Zhao, L., Topping, D.O., Schultz, D.M., Zheng, Z. (2024). Improving urban climate adaptation modeling in the community earth system model (CESM) through transient urban surface albedo representation. *Journal of Advances in Modeling Earth Systems*, *16*(12), e2024MS004380, https://doi.org/10.1029/2024MS004380

Thornton, C., Hutter, F., Hoos, H.H., Leyton-Brown, K. (2013). Auto-WEKA: Combined selection and hyperparameter optimization of classification algorithms. *Proceedings of the 19th ACM SIGKDD international conference on knowledge discovery and data mining* (pp. 847–855). New York, NY, USA: Association for Computing Machinery.

United Nations, D.o.E.a.S.A. (2019). World urbanization prospects 2018 : Highlights. , iv, 30 p.,

Urban, M.C., Alberti, M., De Meester, L., Zhou, Y., Verrelli, B.C., Szulkin, M., . . . Brans, K.I. (2024). Interactions between climate change and urbanization will shape the future of biodiversity. *Nature Climate Change*, *14*(5), 436–447, https://doi.org/10.1038/s41558-024-01996-2

Wang, C., Wu, Q., Weimer, M., Zhu, E. (2021). *FLAML: A fast and lightweight AutoML library.*

Wang, J., Chen, Y., Liao, W., He, G., Tett, S.F.B., Yan, Z., . . . Hu, Y. (2021). Anthropogenic emissions and urbanization increase risk of compound hot extremes in cities. *Nature Climate Change*, *11*(12), 1084–1089, https://doi.org/10.1038/s41558-021-01196-2

Wasala, J., Marselis, S., Arp, L., Hoos, H., Longépé, N., Baratchi, M. (2024). AutoSR4EO: An AutoML approach to super-resolution for earth observation images. *Remote Sensing*, *16*(443), , https://doi.org/10.3390/rs16030443

Xia, X., Fu, D., Shao, W., Jiang, R., Wu, S., Zhang, P., . . . Xia, X. (2023). Retrieving precipitable water vapor over land from satellite passive microwave radiometer measurements using automated machine learning. *Geophysical Research Letters*, *50*(22), e2023GL105197, https://doi.org/10.1029/2023GL105197

Yang, L., Yang, Y., Shen, Y., Yang, J., Zheng, G., Smith, J., Niyogi, D. (2024). Urban development pattern's influence on extreme rainfall occurrences. *Nature Communications*, *15*(1), 3997, https://doi.org/10.1038/s41467-024-48533-5

Yu, J., Sun, Y., Lindley, S., Jay, C., Topping, D.O., Oleson, K.W., Zheng, Z. (2025).

Integration and execution of community land model urban (CLMU) in a containerized environment. , *188*, 106391, https://doi.org/10.1016/j.envsoft.2025.106391

Zhan, C., Xie, M., Lu, H., Liu, B., Wu, Z., Wang, T., … Li, S. (2023). Impacts of urbanization on air quality and the related health risks in a city with complex terrain. *Atmospheric Chemistry and Physics*, *23*(1), 771–788, https://doi.org/10.5194/acp-23-771-2023

Zhao, L., Oleson, K., Bou-Zeid, E., Krayenhoff, E.S., Bray, A., Zhu, Q., … Oppenheimer, M. (2021). Global multi-model projections of local urban climates. *Nature Climate Change*, *11*(2), 152–157, https://doi.org/10.1038/s41558-020-00958-8

Zheng, Z., Fiore, A.M., Westervelt, D.M., Milly, G.P., Goldsmith, J., Karambelas, A., … Dey, S. (2023). Automated machine learning to evaluate the information content of tropospheric trace gas columns for fine particle estimates over india: A modeling testbed. *Journal of Advances in Modeling Earth Systems*, *15*(3), e2022MS003099, https://doi.org/10.1029/2022MS003099

Zheng, Z., Zhao, L., Oleson, K.W. (2021). Large model structural uncertainty in global projections of urban heat waves. *Nature Communications*, *12*(1), 3736, https://doi.org/10.1038/s41467-021-24113-9

Zhou, W., Yu, W., Qian, Y., Han, L., Pickett, S.T.A., Wang, J., … Ouyang, Z. (2021). Beyond city expansion: Multi-scale environmental impacts of urban megaregion formation in China. *National Science Review*, *9*(1), nwab107, https://doi.org/10.1093/nsr/nwab107

Supporting Information

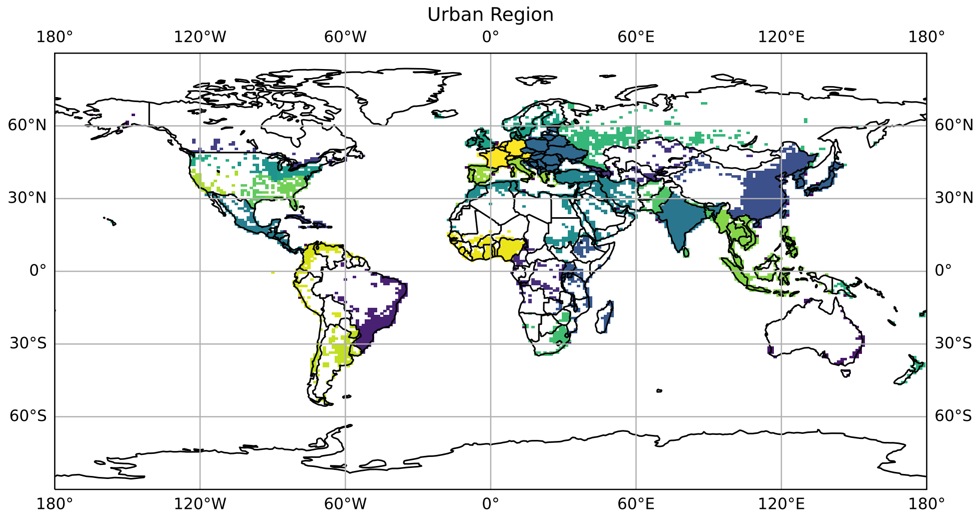

Fig. S1 Urban grids in CESM-LE. Different colors indicate different grid IDs in CESM-LE urban surface dataset.

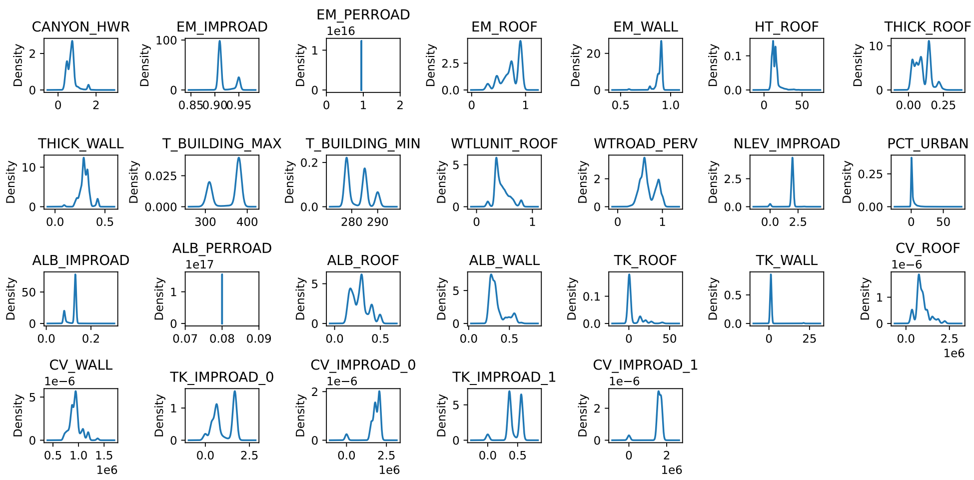

Fig. S2 Original urban surface parameters distribution.

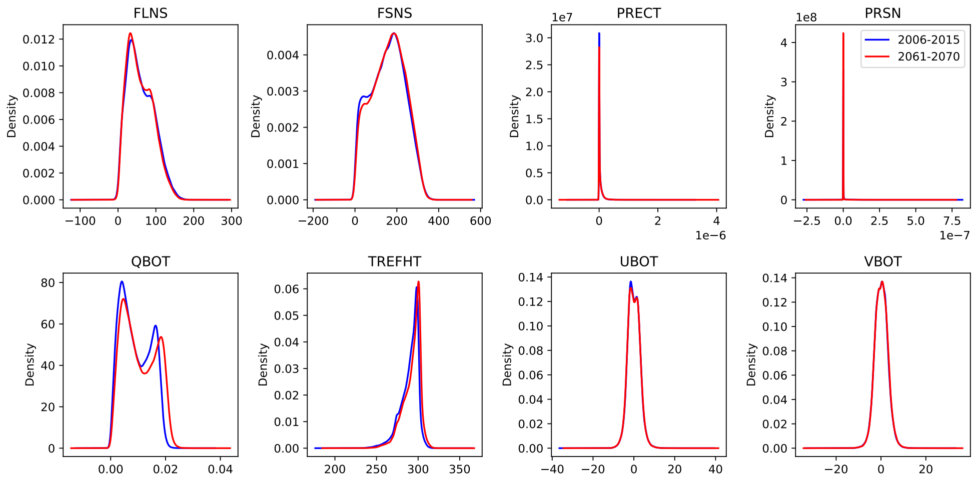

Fig. S3 Atmospheric forcings distribution of training set of 2006–2015 and 2061–2070.

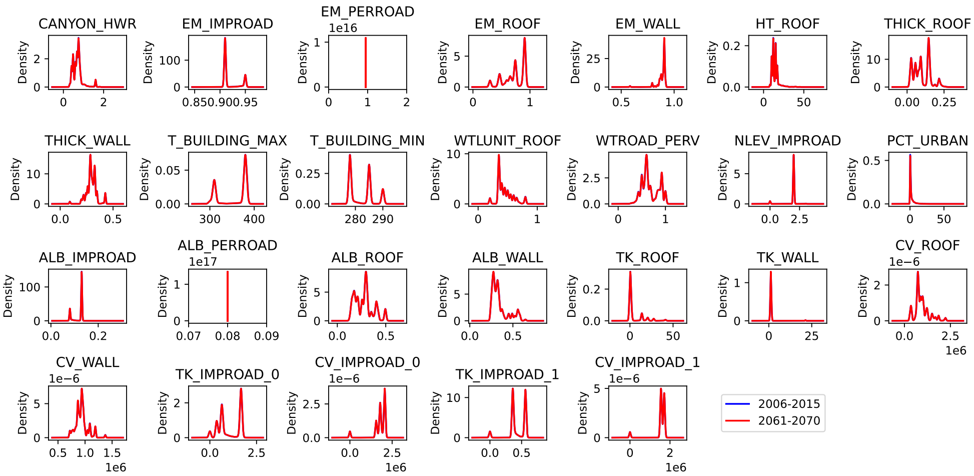

Fig. S4 Urban surface parameters distribution of training set of 2006–2015 and 2061–2070.

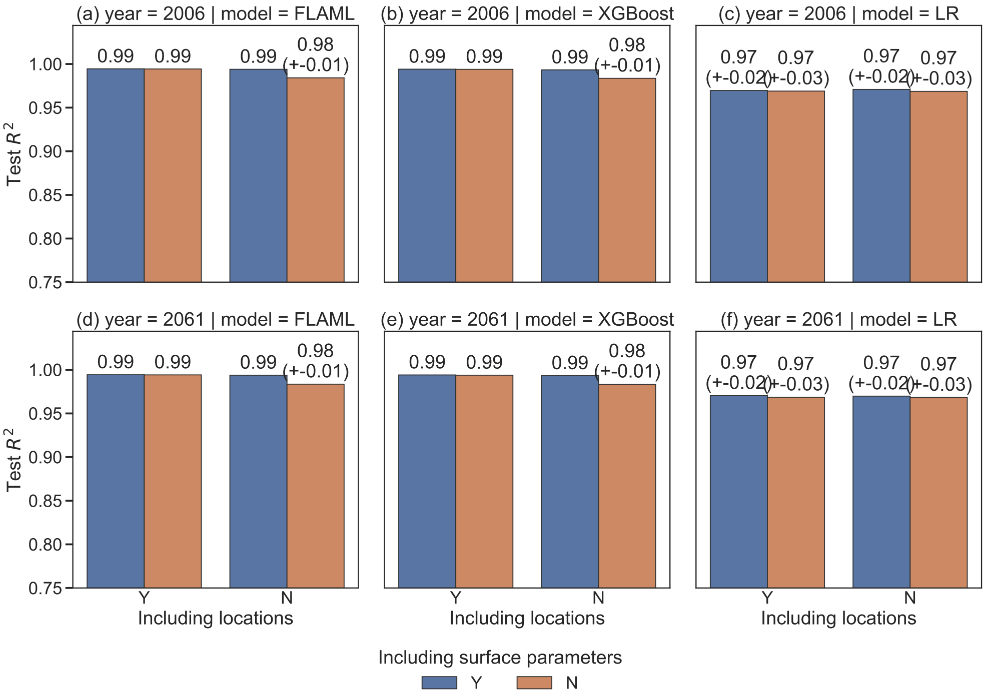

Fig. S5 R square of different models and their differences compared to baseline. (a), (b) and (c) indicate the training set ranges from 2006–2015; (d), (e) and (f) indicate the training set ranges from 2061–2070; (a) and (d) indicate modeling by FLAML; (b) and (e) indicate modeling by XGBoost; (c) and (f) indicate modeling by LR; Y indicates YES (i.e., with LOC/SURF), N indicates NO (i.e., without LOC/SURF). Bar labels in (a) and (d) use the first column as the baseline. Bar labels within the parenthesis in (b) and (e) use the labels in (a) and (d) as the baselines, respectively. Bar labels within the parenthesis in (c) and (f) use the labels in (b) and (e) as the baselines, respectively.

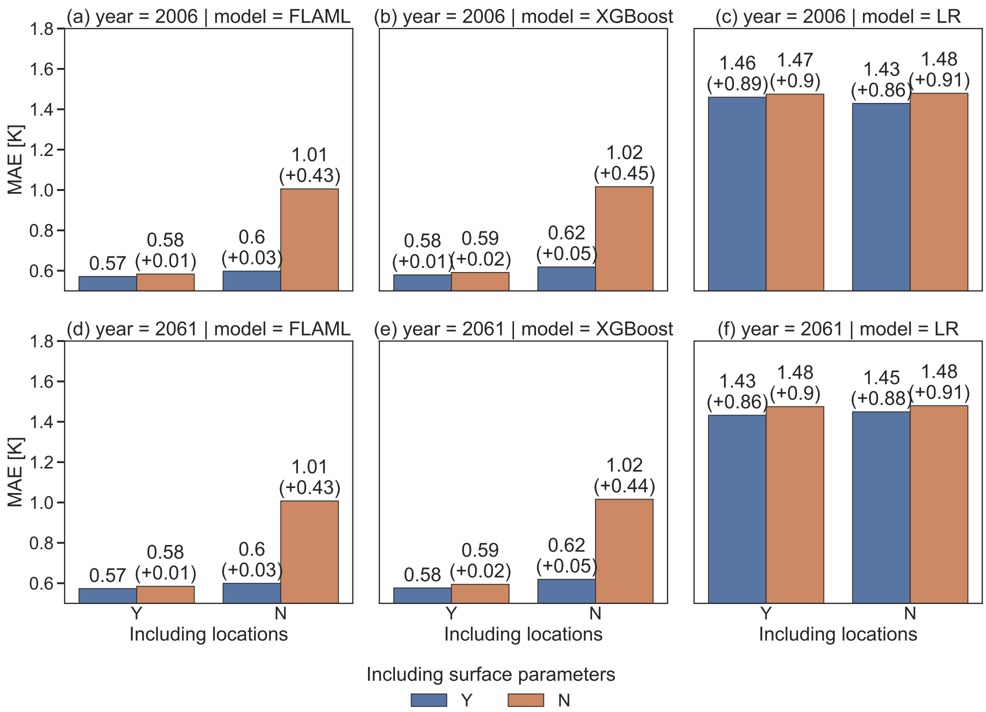

Fig. S6 MAE of different models and their differences compared to baseline. (a), (b) and (c) indicate the training set ranges from 2006–2015; (d), (e) and (f) indicate the training set ranges from 2061–2070; (a) and (d) indicate modeling by FLAML; (b) and (e) indicate modeling by XGBoost; (c) and (f) indicate modeling by LR; Y indicates YES (i.e., with LOC/SURF), N indicates NO (i.e., without LOC/SURF). Bar labels within the parenthesis in (a) and (d) use the first column as the baseline. Bar labels within the parenthesis in (b) and (e) use the labels in (a) and (d) as the baselines, respectively. Bar labels in (c) and (f) use the labels in (b) and (e) as the baselines, respectively.

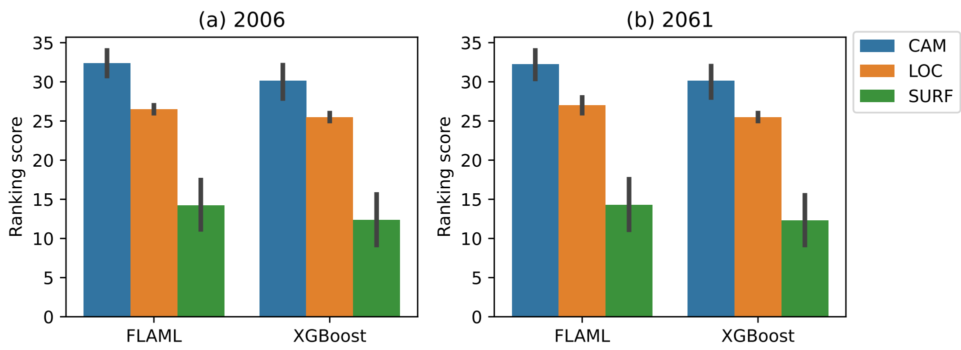

Fig. S7 Average ranking score in three selected categories of different models using tree-based importance. (a) indicates the training set ranges from 2006–2015; (b) indicates the training set ranges from 2061–2070; CAM indicates atmospheric forcing from CAM; LOC indicates locations; SURF indicates urban surface parameters.

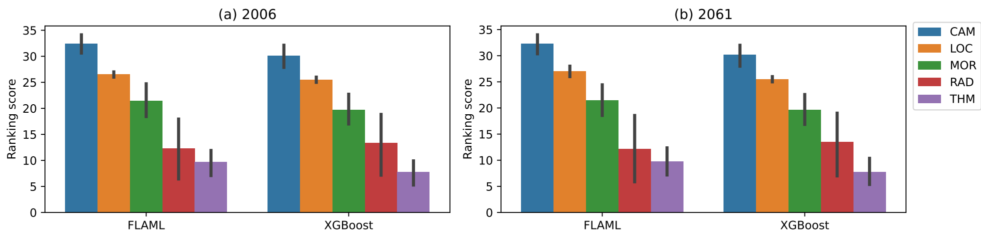

Fig. S8 Average ranking score in five selected categories of different models using tree-based importance. (a) indicates the training set ranges from 2006–2015; (b) indicates the training set ranges from 2061–2070; CAM indicates atmospheric forcing from CAM; LOC indicates locations; MOR, RAD and THM indicate morphological, radiative and thermal urban surface parameters, respectively.

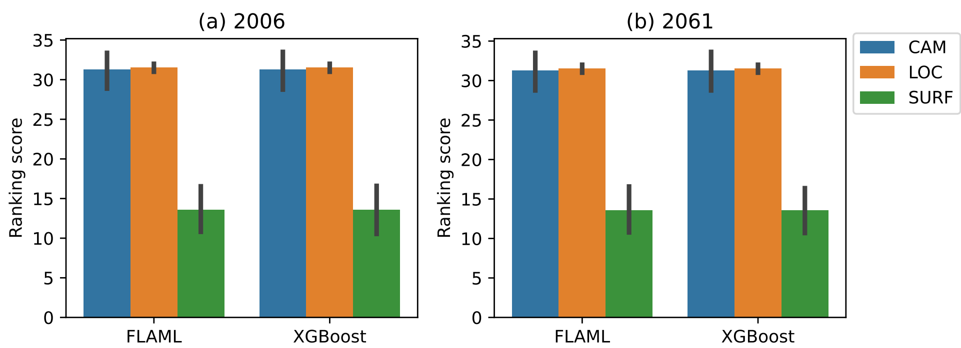

Fig. S9 Average ranking score in three selected categories of different models using permutation importance. (a) indicates the training set ranges from 2006–2015; (b) indicate the training set ranges from 2061–2070; CAM indicates atmospheric forcing from CAM; LOC indicates locations; SURF indicates urban surface parameters.

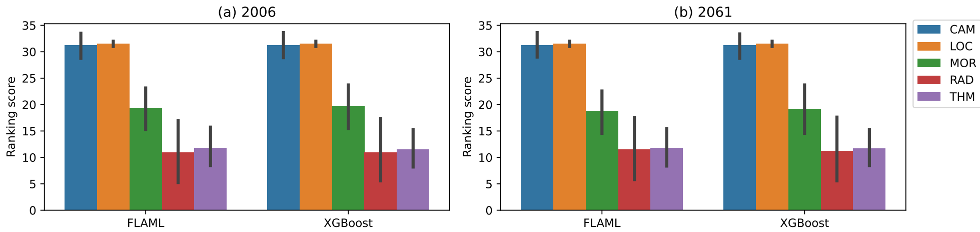

Fig. S10 Average ranking score in five selected categories of different models using permutation importance. (a) indicates the training set ranges from 2006–2015; (b) indicates the training set ranges from 2061–2070; CAM indicates atmospheric forcing from CAM; LOC indicates locations; MOR, RAD and THM indicate morphological, radiative and thermal urban surface parameters, respectively

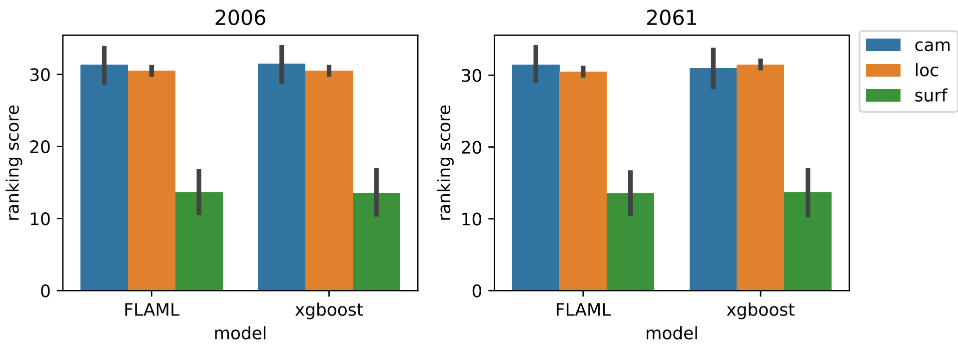

Fig. S11 Average ranking score in three selected categories of different models using permutation importance. (a) indicates the training set ranges from 2006–2015; (b) indicate the training set ranges from 2061–2070; CAM indicates atmospheric forcing from CAM; LOC indicates locations; SURF indicates urban surface parameters.

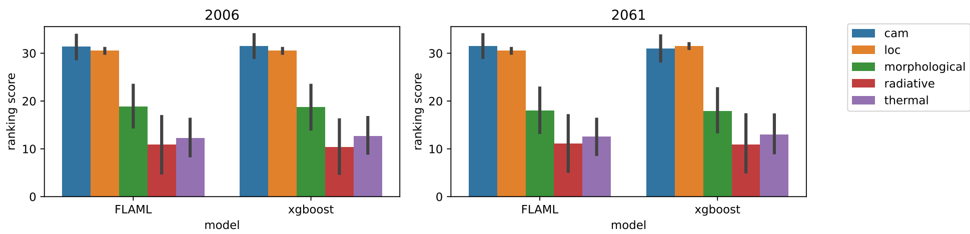

Fig. S12 Average ranking score in five selected categories of different models using SHAP importance. (a) indicates the training set ranges from 2006–2015; (b) indicates the training set ranges from 2061–2070; CAM indicates atmospheric forcing from CAM; LOC indicates locations; MOR, RAD and THM indicate morphological, radiative and thermal urban surface parameters, respectively.